

The Influence of the Confinement Ratio on the Precessing Vortex Core Dynamics in a Counter-Rotating Dual Swirler

Link, Sarah; Dave, K; Eitelberg, Georg; Gangoli Rao, Arvind ; Domenico, Francesca de

DOI

[10.1115/gt2023-101678](https://doi.org/10.1115/gt2023-101678)

Publication date

2023

Document Version

Accepted author manuscript

Citation (APA)

Link, S., Dave, K., Eitelberg, G., Gangoli Rao, A., & Domenico, F. D. (2023). *The Influence of the Confinement Ratio on the Precessing Vortex Core Dynamics in a Counter-Rotating Dual Swirler*. <https://doi.org/10.1115/gt2023-101678>

Important note

To cite this publication, please use the final published version (if applicable). Please check the document version above.

Copyright

Other than for strictly personal use, it is not permitted to download, forward or distribute the text or part of it, without the consent of the author(s) and/or copyright holder(s), unless the work is under an open content license such as Creative Commons.

Takedown policy

Please contact us and provide details if you believe this document breaches copyrights. We will remove access to the work immediately and investigate your claim.

THE INFLUENCE OF THE CONFINEMENT RATIO ON THE PRECESSING VORTEX CORE DYNAMICS IN A COUNTER-ROTATING DUAL SWIRLER

Sarah Link^{1,*}, Francesca de Domenico¹, Kaushal Dave¹, Georg Eitelberg¹, Arvind Gangoli Rao¹

¹Delft University of Technology, Delft, Netherlands

ABSTRACT

Lean-premixed swirl-stabilized combustion is a successful strategy to reduce pollutant emissions. However, these combustion systems are especially prone to thermoacoustic instabilities. The precessing vortex core (PVC) plays a significant role in suppressing or exciting those instabilities. It is therefore necessary to be able to predict the PVC dynamics in different operating conditions. The introduction of alternative aviation fuels like hydrogen in fuel-flexible gas turbines might require changes in the combustor geometry. However, the influence of particular geometric parameters on the PVC dynamics in less conventional combustion chamber configurations is not yet clear. To contribute to the knowledge of PVC dynamics in different combustor geometries, this paper presents an experimental study of the PVC dynamics in isothermal conditions in a counter-rotating dual swirler configuration in different confinement ratios. Additionally, a non-rotating axial air jet can be injected on the center line of the primary swirler as a provision for increased flashback resistance in the reacting case with H₂. PVC frequencies and amplitudes are obtained by spectral proper orthogonal decomposition (SPOD) of time-resolved PIV measurements, and by time-resolved pressure measurements. The study shows that the frequency of the PVC scales with $St_{PVC} = 0.78$, based on the diameter and the bulk velocity of the mixing tube. The PVC frequency is only determined by the conditions in the primary swirler and is fully independent of the amount of airflow going through the secondary counter-rotating swirler. Introducing an axial air jet on the center line decreases the PVC frequency significantly, which can be related to the change in effective swirl number. It is also shown that the smallest combustion chamber diameter results in the highest spectral energy for the PVC mode for all investigated points, hence the PVC motion is the strongest. Meanwhile, the biggest combustion chamber diameter shows the weakest pressure fluctuations. The results obtained in this study provide evidence that the periodic oscillations arising in the swirling flow field can

be predicted and follow a Strouhal scaling independent of the geometry, even for more unconventional configurations.

Keywords: Precessing vortex core, Counter-Rotating swirler, Confinement ratio

NOMENCLATURE

Roman letters

A	Cross section [m ²]
AAI	Axial air injection
c	Confinement ratio [-]
D	Diameter [mm]
f	frequency [Hz]
IRZ	Inner recirculation zone
l	Block length for the DFT
m	Number of PIV snapshots
n_s	Number of data points per snapshot
ORZ	Outer recirculation zone
p	Pressure [Pa]
r	Radius [mm]
U	Velocity [m/s]
x, y	Cartesian coordinates

Greek letters

ϕ	Tip vane angle [rad]
χ	Axial air injection [%]
ψ	Blockage factor

Dimensionless groups

Sw	Swirl number, $G_{\Theta}/(G_x \cdot R)$
St_{PVC}	Strouhal number, $f_{PVC}/(D \cdot U_{\infty})$

Superscripts and subscripts

AAI	Axial air injection
CC	Combustion chamber
MT	Mixing tube
∞	bulk value mixing tube
$\hat{\cdot}$	Fourier transform
\cdot'	Fluctuating part

*Corresponding author: S.J.Link@tudelft.nl

Documentation for asmeconf.cLs: Version 1.32, February 24, 2023.

1. INTRODUCTION

Lean premixed combustion is a widely used approach to reduce NO_x emissions. The excess air lowers the temperature, and consequently reduces the thermal NO_x . Swirl stabilized combustion is state-of-the-art in modern gas turbines to obtain an effective mixing between the fuel and the oxidizer. However, swirling flames are prone to combustion instabilities [1], often caused by the coupling of the unsteady heat release and the resonant frequencies of the combustor. The swirl number Sw is defined as the ratio of the axial flux of tangential momentum to the axial flux of axial momentum. Strongly swirling flows are characterised by substantial radial and axial pressure gradients: above a critical swirl number, these might result in the formation of an inner recirculation zone (IRZ) [2]. Due to low velocities and the transport of radicals from product gases the IRZ, flames can be stabilized even in lean conditions.

For conventional fuels, two or multi-stage swirlers have been proven to be beneficial for mixing performance and pollutant generation. Counter-rotating swirlers create a stronger and shorter recirculation zone [3], which allows for a more compact combustion chamber design. For spray flames, this configuration results in finer droplets and better mixing of fuel and oxidizer [4].

However, in swirling flows the inner shear layer between the swirling jet and the IRZ is prone to develop a single helical (azimuthal wavenumber $m = 1$), self-induced hydrodynamic instability known as precessing vortex core (PVC) [5, 6]. While in the non-reacting flow cases, a PVC is always present above a critical swirl number [7], in reacting cases its presence is strongly related to the transition of different flame shapes, more precisely to the lift-off of the flames from the injectors [8, 9]. The PVC originates from a region of absolute instability in the inner shear layer, then grows to the outer shear layer, and finally might impose its frequency on the whole flow field [10]. It was shown that the frequency of the PVC scales linearly with the mass flow rate in both non-reacting and reacting conditions [9, 11]. The PVC significantly influences the flame dynamics. For example, it affects the flame-vortex interaction [12] and it can cause global heat release oscillations if the flow field is not completely symmetric. However, the interaction of the PVC with thermoacoustic instabilities is still not fully understood, as opposite behaviours have been observed. Steinberg *et al.* [13] showed that PVC can contribute to the excitation of thermoacoustic instabilities for a fully premixed combustor. Results from the PRECCINSTA GTMC burner operated at elevated pressure in a partially premixed configuration revealed that the PVC plays a critical role in sustaining the thermoacoustic instabilities [14]. However, recent studies demonstrated that the actuation of the PVC in conditions where naturally no PVC is present can be exploited to suppress thermoacoustic instabilities [15, 16]. By increasing the thickness of the shear layer, the PVC can suppress the receptivity of the shear layer to external disturbances. This leads to a much smaller growth rate after a disturbance in the shear layer when a PVC is present [17]. Additionally, the PVC increases the level of turbulent kinetic energy, which can significantly improve the mixing of fuel and oxidizer for partially premixed configurations [18, 19]. However, slight increases in NO_x levels have also been observed for premixed flames, as the

flame wrinkling can generate longer residence times [20].

This paper focuses on understanding the PVC dynamics of a dual-stage swirler designed to be operable with hydrogen and kerosene, in non-reacting conditions. The introduction of an axial air injection (AAI) jet is employed in the primary swirler, as this has been proven to be a promising concept to decrease the flashback propensity in swirl stabilized hydrogen flames [21, 22]. Since previous studies for single-stage configurations have shown a reliable scaling of the PVC frequency from non-reacting conditions to reacting conditions [9], results obtained from isothermal conditions are expected to provide valuable insights to understand the PVC dynamics in such configuration.

Moreover, the effect of confinement ratio and outlet boundary conditions are analysed to further understand and characterise the behaviour of the combustor.

The confinement ratio in radial direction strongly alters the flow field characteristics, as the confinement increases the recirculated mass flow in the inner recirculation zone, which strongly affects the flame [23]. Moreover, the confinement of the flow can double the turbulent kinetic energy with respect to unconfined configurations [24], with an increasing trend for smaller combustion chamber diameters. Smaller diameters additionally decrease the size and length of the inner recirculation zone in streamwise direction [25]. This offers advantages in designing compact combustion chambers. However, for reacting cases, this might also lead to a blow-off limit at a higher equivalence ratio due to higher strain rates and higher flow velocities [26, 27]. Based on these previous findings, the confinement ratio has a significant influence on the strength of the recirculation zone and the shear layer and is therefore expected to influence the precessing vortex core.

Additionally, AAI has been shown to significantly affect the flow field and the PVC dynamics [28]. The effect of the confinement ratio on the PVC dynamics in combination with AAI is still unknown, and will also be investigated in this paper. According to the author's knowledge, no PVC studies have been performed in a counter-rotating swirler with different confinement ratios. To evaluate the influence of the secondary swirler separately from the influence of the confinement ratio, additional measurements are performed with only the primary swirler.

The paper is organized as follows: Section 2 gives an overview of the experimental set-up and the measurement techniques. Section 3 discusses the findings of the PVC dynamics for the single and the dual-stage swirlers. Finally, section 4 presents the most important findings of this study.

2. EXPERIMENTAL SET-UP

Geometry. Experiments were performed in non-reacting conditions in a dual counter-rotating swirler in a cylindrical combustion chambers with different confinement ratios at the exit. Fig. 1 shows the schematic of the set-up. Both swirlers (inner and the outer counter-rotating swirlers) have a geometric swirl number of 1.1. For helical swirlers, this swirl number is defined as [29]

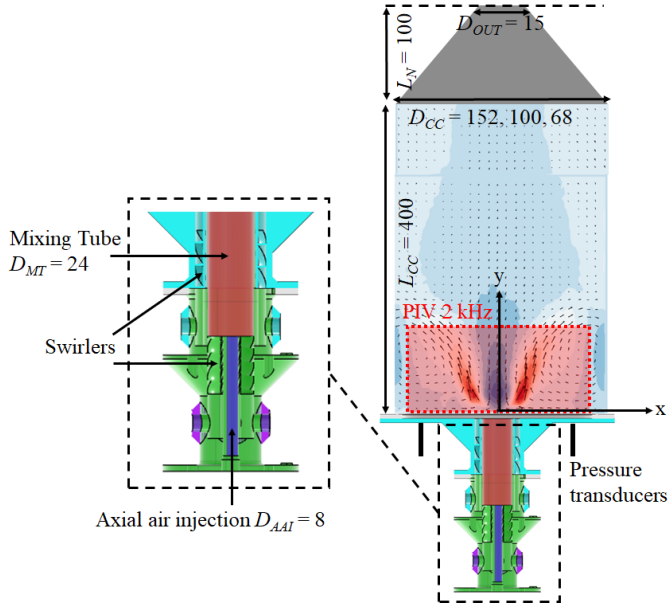


FIGURE 1: SCHEMATIC OF THE EXPERIMENTAL SET-UP, LENGTH SPECIFICATIONS IN MM

$$Sw = \frac{G_{\Theta}}{R_n \cdot G_x} = 0.5 \frac{1}{1 - \psi} \frac{1 - (R_h/R_n)^4}{1 - (R_h/R_n)^2} \tan(\phi_0) \quad (1)$$

with G_{Θ} being the axial flux of tangential momentum, G_x the axial thrust, ψ the blockage ratio, ϕ_0 the tip vane angle and R_n and R_h respectively the outer and hub radius. The inner swirler is winding around the axial air injection (AAI) tube through which a non-rotating air jet gets injected. The mixing tube connects the swirler with the combustion chamber.

The combustor is designed for an operating power of 11 kW and an equivalence ratio of $\phi = 0.75$. This work describes the experimental characterization performed in non-reacting conditions, with a bulk velocity of $U_{\infty} = 9.8$ m/s and $Re = 15900$ for the baseline case. The mixing tube and the AAI tube have an inner diameter of respectively $D_{MT} = 24$ mm and $D_{AAI} = 8$ mm. The combustion chamber has a length of $L_{CC} = 400$ mm and variable inner diameter D_{CC} (152 mm, 100 mm and 68 mm) resulting in three different confinement ratios

$$c = \frac{A_{CC}}{A_{MT}} = 40, \quad 17, \quad 8 \quad (2)$$

To allow control over the outlet boundary conditions and to quantify the influence on the flow fields, experiments were additionally performed with a converging nozzle at the outlet of the combustion chamber (see Fig. 1). For all the D_{CC} , the nozzle has a length of 100 mm and an outlet diameter D_{out} of 15mm.

Operating conditions. Measurements were carried out at different operating conditions, shown in table 1, by varying the air mass flows of the primary swirler \dot{m}_{prim} , secondary swirler \dot{m}_{sec} and the axial air injection \dot{m}_{AAI} . To better evaluate the influence of the secondary swirler, some initial measurements were performed with the primary swirler only, setting the baseline

case for the study to $\dot{m}_{prim,base} = 250$ l/m. The effect of axial air injection (AAI) for the primary swirler was then evaluated. Since the combustor is designed to operate on H_2 in the reacting cases, AAI is used as a strategy to decrease the propensity to flashback. For the cases with AAI, the total mass flow is kept constant and the percentage of AAI is given with

$$\chi = \frac{\dot{m}_{AAI}}{\dot{m}_{total}} \quad \text{with} \quad \dot{m}_{total} = 250 \text{ l/m} \quad (3)$$

Additionally, table 1 shows whether the results are shown for the configuration with outlet nozzle or without.

TABLE 1: OPERATING POINTS, UNIT OF THE MASS FLOWS \dot{m} IS L/M

Experiment	\dot{m}_{prim}	\dot{m}_{sec}	χ [%]	open	nozzle
Baseline case	250	-	-	✓	✓
Single swirler	150-350	-	-		✓
Dual swirler	250	0 - 250	-	✓	✓
χ (AAI)	225-250	-	0 - 10		✓

Measurement techniques. Time-resolved PIV measurements at 2 kHz were performed at the center plane (see Fig. 1). The particles (1.0 μm diameter DEHS oil droplets), injected from the two swirling air streams, were illuminated with a dual pulsed Nd:YAG laser (Continuum MESA PIV 532-120-M). The laser sheet was around 2.5 mm thick. The flow fields were recorded with two Photron Fastcam SA-1 cameras with a sensor size of 1024 x 1024 pixels, equipped with a 60 mm lens. This resulted in a resolution of 14.6 pix/mm. One of the cameras looked at an angle of 11° at the field of view, which caused a slight error in the absolute velocities. The velocity fields were post-processed with the PIV software LaVision Davis 8.0. A cross-correlation algorithm was applied with a final interrogation window of 24x24 and 50% overlap. The velocity fields were averaged over $N = 2000$ image pairs and normalized with the bulk velocity U_{∞} in the mixing tube. The random error in the velocities is given by U_{rms}/\sqrt{N} , where U_{rms} is the root-mean-square of the velocity. With the sample size of 2000 images this resulted in a velocity uncertainty of around 2% of U_{rms} . In the plots of this paper, all the length scales are normalized with the mixing tube diameter D_{MT} .

Additional to the PIV measurements, two differential pressure sensors were positioned at $r = 2.7$ mm and $r = -2.7$ mm on the base plate of the combustor. The pressure data were acquired with a HoneyWell TruStability differential pressure transducer (accuracy: 0.25% FS, sampling frequency: 2 kHz, range ± 0.6 kPa).

Data processing and analysis. A spectral proper orthogonal decomposition (SPOD) was applied separately on the x-component u_x and y-component u_y of the velocity data. The SPOD modes are presented in u_x velocity since the helical (asymmetric) structure of the PVC can be identified easily by the axis-symmetric patterns in the modes [6]. As demonstrated in Terhaar et al. [30], a proper orthogonal decomposition of the flow

field data in Cartesian coordinates results in a symmetric pattern when computing the modes of the transversal velocity u_x or the through-plane vorticity ω_z . If they are computed in cylindrical coordinates, the modes are skew-symmetric. The SPOD is derived from a space-time POD and offers the advantage of a coherent evolution of the modes in space and time. SPOD on a two-dimensional flow field only can only give an indication of the 3D structure in the two-dimensional view. However, it does give information about the correlation of the flow in the 2D plane. The resulting PVC patterns in a 2D plane have been clearly identified by previous authors [6]. Therefore, and due to the rotational symmetry of swirling flows, valid conclusions on the PVC structure can be drawn from an analysis of the 2D flow field.

The analysis was performed with the open-source MATLAB function SPOD [31]. The data matrix of the fluctuating x-component U'_x consists of m (number of snapshots) columns with the dimension of $n_s = N_x \cdot N_y = 29\,241$ (number of data points in x- and y-direction). The matrix U'_x of the fluctuating velocities gets determined by removing the average velocities of every column from their respective column in the velocity matrix.

$$U'_x = \begin{bmatrix} u'_{x,11} & \dots & u'_{x,1m} \\ u'_{x,21} & \dots & u'_{x,2m} \\ \dots & \dots & \dots \\ u'_{x,n_s1} & \dots & u'_{x,n_sm} \end{bmatrix} = [u'_{x,1}, u'_{x,2}, \dots, u'_{x,m}] \in \mathbb{R}^{n_s \times m} \quad (4)$$

For the Discrete Fourier Transform (DFT) applied to the matrix U'_x , the columns of U'_x got divided into blocks with a length of $l = 512$. Each n^{th} block ($n_s \times l$) and its Fourier transform can be written as

$$U'_x^{(n)} = [u'_{x,1}^{(n)}, u'_{x,2}^{(n)}, \dots, u'_{x,l}^{(n)}] \quad (5)$$

$$\underline{DFT} \quad \hat{U}'_x^{(n)} = [\hat{u}'_{x,1}^{(n)}, \hat{u}'_{x,2}^{(n)}, \dots, \hat{u}'_{x,l}^{(n)}]$$

A 50% overlap resulted in $n_b = 6$ blocks with a size of $n_s \times l$. A Hanning window filtering got applied to the data, which resulted in a frequency resolution of 4 Hz. After the DFT, the data are present at 257 discrete frequencies f . The Eigenvalue analysis is performed on one frequency at a time, with the data matrix written as following

$$\hat{U}'_{x,f} = [\hat{u}'_{x,f}^{(1)}, \hat{u}'_{x,f}^{(2)}, \dots, \hat{u}'_{x,f}^{(n_b)}] \quad (6)$$

The cross-spectral density tensor is determined as

$$\hat{C} = \frac{1}{n_b - 1} \hat{U}'_{x,f} \hat{U}'_{x,f}^T \quad (7)$$

Finally, the eigenvalues and eigenvectors are computed following the traditional POD procedure [32]. For a more detailed description of the SPOD methodology, the reader is referred to the work of Schmidt *et al.* [33].

For the pressure measurements, a Fast Fourier Transform (FFT) of $\Delta p = p_2 - p_1$ provides the spectrum of the pressure fluctuations. Applying the FFT to the difference between the two pressure signals ensures that the pressure fluctuations are not caused by a symmetric structure, but by an asymmetric structure

such as the PVC. The pressure signal recorded for 5 seconds was divided into blocks with a length of 4000 samples. A Hanning window filtering with 50% overlap resulted in a final frequency resolution of 2Hz. The difference on the frequency of the PVC obtained from the pressure measurements and the frequency obtained from the SPOD data is below 3%.

3. RESULTS

The main goal of this work is to evaluate the behavior of the PVC in a double swirler injector, with the addition of axial air injection. Additionally, the effects of the confinement ratio and of the outlet boundary conditions are investigated. The results are organised as follows. First, the baseline case (single-stage swirler) is investigated. In this configuration, the impact of the confinement ratio and of the outlet nozzle on the PVC dynamics are analyzed (Section 3.1). For the dual-stage swirler, the measurements are presented with and without nozzle, in order to verify the validity of the results independently of the outlet boundary conditions (Section 3.3). Finally, the influence of axial air injection on the PVC dynamics is evaluated (Section 3.4).

3.1 Single swirler

In this section, the flow field and corresponding PVC frequencies obtained in the baseline configuration (single swirler and no axial air injection) are analyzed.

3.1.1 Confinement ratio investigation. The effect of the confinement ratio is investigated in this section. The outlet of the combustion chamber remains open, meaning that no nozzle is attached to the exit of the combustion chamber. The analysis is performed by the primary mass flow \dot{m}_{prim} Fig. 2 shows the average flow fields for the streamwise velocity for different confinement ratios. Confining the swirling flow increases the length and the width of the IRZ and additionally results in the creation of outer recirculation zones. Moreover, the streamwise velocity in the jet decreases due to the wider spreading of the swirling jet. This can also be observed in Fig. 3, where the streamwise velocity is plotted at two different streamwise locations. The jet velocity also decreases for lower confinement ratios, however, it shows the lowest values for $c = 17$ instead of $c = 8$. This can be related to the visible slightly wider opening of the swirling jet for $c = 17$.

A smaller combustion chamber diameter causes a widening of the recirculation zone and a wider and longer zone of high negative axial velocities in the IRZ. Nevertheless, at $y/D_{MT} = 0.7$, the biggest confinement ratio still shows the highest negative streamwise velocities. Under the assumption of rotational symmetry, the wider recirculation zones and high negative velocities indicate a higher recirculated mass flow. While for $y/D_{MT} = 0.7$ this difference does not seem striking, for $y/D_{MT} = 1.4$ the smallest diameter shows higher negative velocities and a wider recirculation zone. This is contradictory to the findings in [25], where small confinement ratios result in a smaller zone of high negative velocities. However, this is expected to be caused by the different swirler configurations. The authors in [25] chose a diverging-converging mixing tube, which in their case prevents the formation of outer recirculation zones. Since a low confinement ratio results in a lower recirculated mass flow, this necessarily

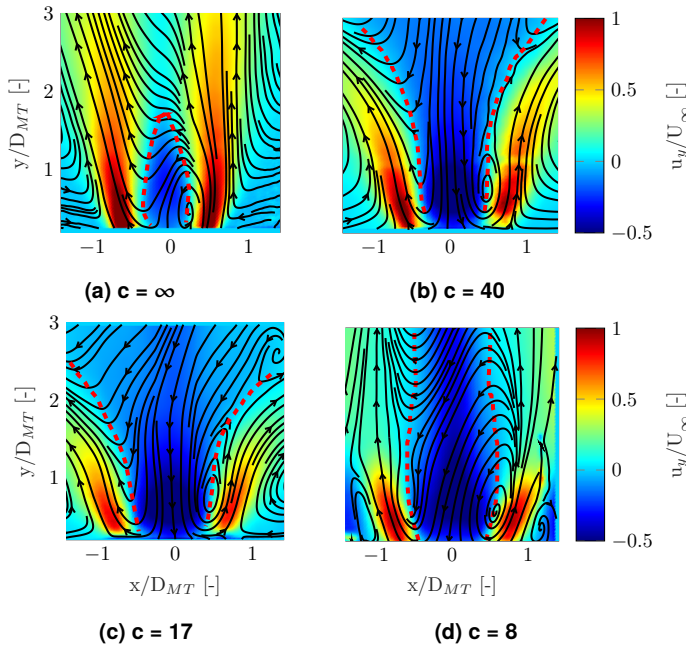


FIGURE 2: AVERAGE STREAMWISE VELOCITY u_y FIELDS IN DIFFERENT CONFINEMENT RATIOS c , DASHED LINES INDICATES ZERO u_y LINE

involves a smaller recirculation zone with high negative velocities. For the present configuration, the mass flow gets recirculated through the outer recirculation zones, with a decreasing size for lower c . Therefore, as compared to Fu *et al.* [25], the velocities in the IRZ can not directly be related to the amount of recirculated mass flow.

3.1.2 Analysis of the PVC behaviour. In Fig. 4 the PVC frequency f and the amplitude $|P(f)|$ obtained from the pressure spectrum are presented for different confinement ratios by varying the injected mass flow rate in the primary swirler. In addition, a line with constant Strouhal number $St_{PVC} = \frac{f \cdot D_{MT}}{U_\infty}$ of 0.78 is shown. This scaling is in good agreement with the frequency scaling for a swirl number of $Sw = 1.1$ in non-reacting conditions obtained in previous studies [9, 11], where a St_{PVC} of around 0.75 was reported. This corresponds to the previously reported Reynolds' law of similarity, which states independence of the St number for high enough Reynolds numbers [11]. The unconfined configuration follows this constant St number line almost perfectly. In the confined cases, the frequencies slightly deviate below the theoretical predictions by increasing \dot{m}_{prim} . This shows that the frequency of the PVC is only marginally affected by the level of confinement. The pressure amplitude of the PVC, however, varies significantly with the level of confinement, with higher amplitudes for lower confinement ratios. It can be observed that for the confined cases, the amplitude increases for higher mass flow rates and drops for all the cases at 300 l/m. At this operating condition, the PVC frequency matches the first resonant frequency of the open cylindrical combustion chamber. The authors speculate that at this operating point, a part of the PVC energy gets absorbed by the vibration of the combustion chamber. This hypothesis of destructive interaction between the

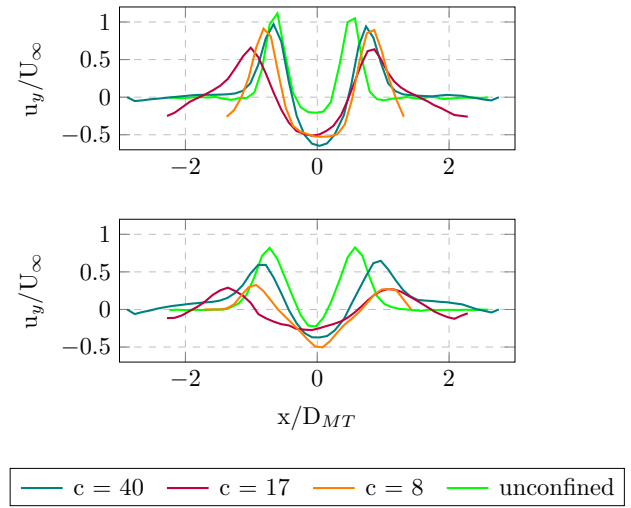


FIGURE 3: STREAMWISE VELOCITY PROFILES AT $Y/D_{MT} = 0.7$ (TOP) AND $Y/D_{MT} = 1.4$ (BOTTOM) FOR DIFFERENT CONFINEMENT RATIOS

PVC and the acoustics of the chamber is further corroborated by the fact that this decrease in the PVC strength is not observed in the unconfined case. However, the current data does not allow for a more detailed analysis, therefore further experiments are needed to verify this speculation.

The change in pressure amplitude $\Delta|P(f)|$ between $c = 40$ and $c = 8$, however, stays constant throughout the whole range of \dot{m}_{prim} . The amplitude for the unconfined case does not show a significant increase but remains more constant compared to the confined cases. The change in pressure amplitude with a smaller confinement ratio is expected to be a result of the change in the size of the outer recirculation zones (ORZ). As the pressure taps are installed at the baseplate, they measure the pressure fluctuations in the ORZ. The mass flow in the ORZ presumably serves as a damper of the PVC pressure fluctuations, consequently, a bigger ORZ with more recirculated mass flow would dampen the amplitude more.

When looking at the spectral energy and the corresponding modal energy of the first SPOD mode from the PIV data (Fig. 5), one observes that $c = 8$ shows much higher energy than $c = 40$. This indicates that the increase in pressure fluctuations for $c = 8$ in the ORZ is also caused by a stronger PVC motion. As shown by Manoharan *et al.* [17] the growth rate of the PVC decreases with the thickness of the shear layer. Under the assumption that the growth rate of the PVC is an indication of the increasing amplitude of the PVC [34], an increase in shear layer thickness causes a decrease in pressure fluctuations. Due to the higher levels of recirculated mass flow in the IRZ, it is expected that the shear layer thickness decreases for the lowest confinement ratio. This is a plausible explanation for the higher energy of the first SPOD mode.

The spectral peaks at the harmonics of the PVC are described by some authors as a well-known artifact of the Discrete Fourier Transform (DFT) component of the SPOD algorithm [35], others describe the harmonics being a result of non-linearity effects [7]. However, the underlying mechanism resulting in the harmonics is not relevant to the analysis presented

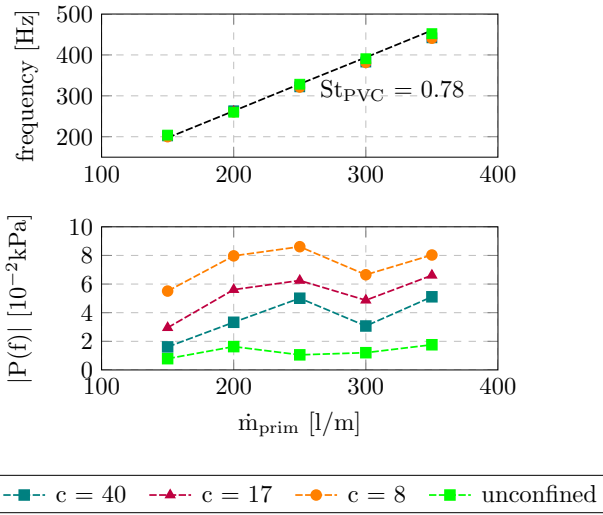


FIGURE 4: PVC FREQUENCIES (TOP) AND PRESSURE AMPLITUDES (BOTTOM) FOR THE SINGLE SWIRLER AT DIFFERENT \dot{m}_{prim}

in this paper.

Fig. 6 shows the normalized spatial amplitude distribution of the real part of \hat{u}_x for the three different confinement ratios. The values of each confinement ratio have been normalized with the same amplitude of 0.03. The flow patterns represent the coherent helical structures of the PVC and can therefore indicate the size and shape of the PVC. It can be observed that the opening angle, indicating the helix radius of the PVC, follows the same trend as the opening angle of the swirling jet, as previously shown in Fig. 2. This is expected since the PVC is wrapped around the IRZ and therefore changes its shape according to the shape of the IRZ. It can also be observed that the extent of the helical structure in streamwise direction is the longest for the unconfined case and the shortest for the smallest confinement ratio. This is expected to be a consequence of the wider helix radius for decreasing confinement ratios up to $c = 17$. This decreases the angular velocity in the streamwise direction according to the conservation of angular momentum. Consequently, this decreases the length of influence in streamwise direction, where the PVC motion can dominate the flow field motion. Therefore the PVC breaks and disappears further upstream. For $c = 8$ it is expected that due to the high level of confinement, the PVC interacts with the wall at a short streamwise distance from y/D_{MT} . Moreover, also the helix pitch decreases for decreasing confinement ratios. As shown by Favrel *et al.* [36], if the swirl number stays constant and the helix radius increases, the helix pitch has to decrease. The helix of $c = 8$ shows a smaller helix pitch and a smaller helix radius than the one of $c = 17$. This would indicate a lower swirl number for $c = 8$, which is a consequence of the strong interaction with the combustion chamber wall. Based on these findings, it is expected that lower confinement ratios up to a critical value $c_{critical}$ result in a lower helix pitch and a higher radius. Below $c_{critical}$ the effect of the interaction of PVC and combustion chamber wall seems dominating, which suggests a decrease in the swirl number.

In this section it was shown that the PVC frequency for

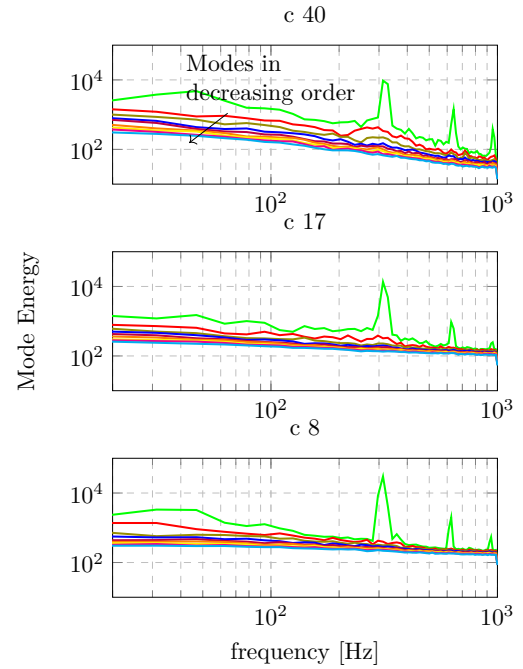


FIGURE 5: MODE ENERGY SPECTRUM FOR DIFFERENT CONFINEMENT RATIOS c

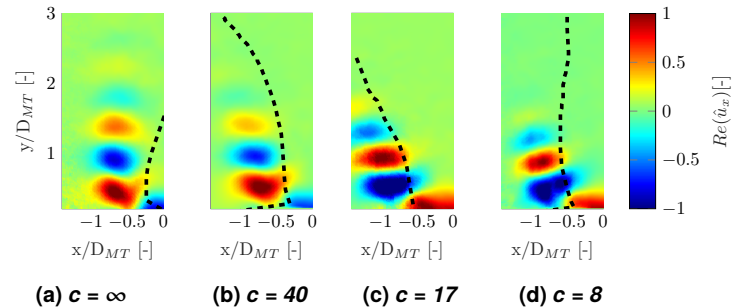


FIGURE 6: NORMALIZED TRANSVERSAL VELOCITY COMPONENT \hat{u}_x (REAL PART) FROM THE SPOD MODE 1, DASHED LINES INDICATES ZERO u_y LINE

the investigated configuration scales as predicted with $St_{PVC} = 0.78$. The pressure amplitude increases with a decrease in the confinement ratio, which is a consequence of the greater damping due to the larger volume in the bigger combustion chambers.

3.1.3 Effect of the outlet boundary condition. Previous studies have shown a significant influence of the outlet boundary conditions on the overall flow field and the PVC dynamics [34, 37]. To evaluate the change in flow field due to different boundary condition for this set-up, the baseline case was tested with and without a converging nozzle at the outlet for the three confinement ratios. The analysis presented here is performed on the single-stage configuration, to decouple the effect of the nozzle from the secondary mass flow, \dot{m}_{sec} , on the PVC.

The diagrams in Fig. 7 display the pressure spectra of the baseline case for the different confinement ratios. The frequency and pressure amplitude values for the corresponding cases with outlet confinement are marked with a circle. For all the confine-

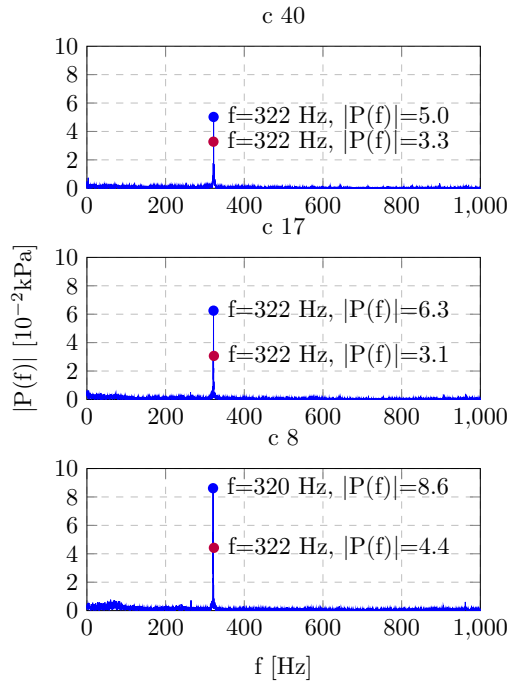


FIGURE 7: PRESSURE SPECTRUM FOR THREE DIFFERENT CONFINEMENT RATIOS WITH (●) AND WITHOUT OUTLET CONFINEMENT (●).

ment ratios, the pressure amplitude decreases for the configurations with outlet contraction. It is noticeable that the amplitude decreases more as the confinement ratio decreases. This decrease in amplitude is caused by the thickening of the inner shear layer caused by the outlet contraction, which weakens the driving force of the coherent PVC structure [34]. This can be observed in Fig. 8, which plots the average streamline velocity for two confinement ratio, with and without the outlet contraction. The cases with outlet contraction generate an accelerating flow in the forward direction and decrease the maximum negative streamwise velocity. This behavior was also reported by previous works [37–39]. It can be noticed that in the smallest diameter case (Fig. 8c) the outlet contraction has a stronger influence compared to the biggest diameter case (Fig. 8d), despite the higher negative velocities in the IRZ for the case without outlet contraction. Esucier *et al.* [40] related the appearance of this flow structure in swirling flows to the ability of the flow to allow upstream travel of disturbances. This characteristic of the flow is associated with the criticality theory, which describes the sensitivity of the flow fields for subcritical flows. A metric for criticality is the remaining swirl on the outlet of the combustor [38].

Based on the criticality theory, the lowest confinement ratio should exhibit a higher effective swirl number at the outlet of the nozzle. From the results of previous studies, the conicity of the nozzle influences the swirl decay in the nozzle significantly [41]. A lower conicity, as in the case of the lowest confinement ratio, reduces the swirl decay compared to a nozzle with high conicity. Under the assumption of a constant swirl number at the entry of the nozzle for all the confinement ratios c , this would result in a higher remaining swirl number at the nozzle exit for the smallest

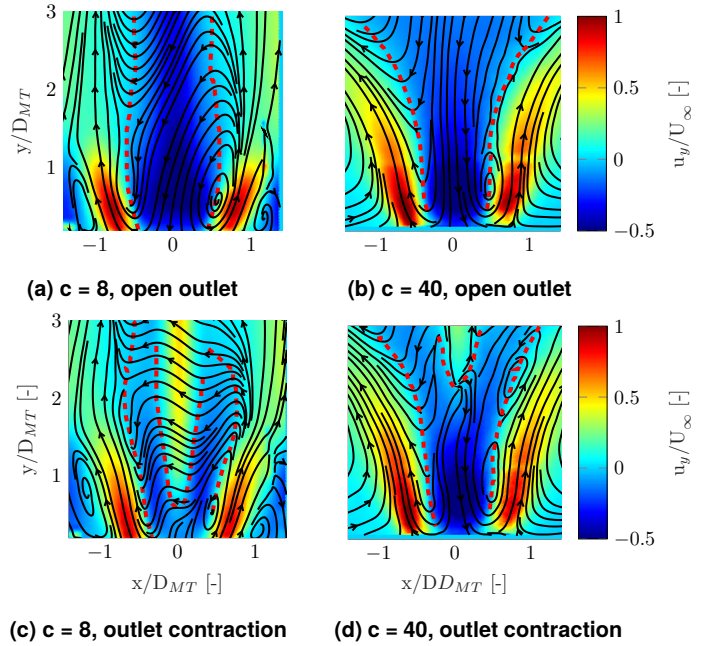


FIGURE 8: AVERAGE STREAMWISE u_y VELOCITY FIELDS, DASHED LINES INDICATES ZERO u_y LINE

c . This also explains the changes in pressure amplitude in Fig 7: the lowest confinement ratio $c = 8$ shows the highest change in pressure amplitude due to the strongest influence of the forward jet in the flow field.

The changes in the IRZ are also more prominent for the smallest diameter, which is characterized by a change in the opening angle of the swirling jet and the magnitude of negative streamwise velocities. Furthermore, the size of the outer recirculation zones has slightly increased. These parameters are mostly unaffected for the biggest diameter.

In Fig. 9 the differences between the first SPOD mode for $c = 8$ with and without outlet contraction are shown. The PVC shows a wider opening angle for the open outlet case, which coincides with the opening of the swirling jet. Moreover, the outlet contraction causes more dispersed edges of the coherent structures (Fig. 9b). This indicates a strong influence of the jet formed due to the outlet contraction on the PVC shape. In this section, it was shown that the flow field in the combustion chamber is sensitive to the outlet boundary condition. The PVC frequency is unaffected by the outlet conditions, however the change in pressure amplitude with outlet nozzle strongly depends on the confinement ratio.

3.2 Dual counter-rotating swirler

This section evaluates the influence of the secondary swirler on the PVC dynamics. The analysis is performed both with and without outlet boundary conditions. This allows a generalization of the findings for both configuration, as it was previously demonstrated that the exit nozzle has a non-negligible effect on the PVC behaviour. The analysis is performed by varying the secondary air flow and the confinement ratio, while keeping the primary mass flow rate fixed at 250 l/m.

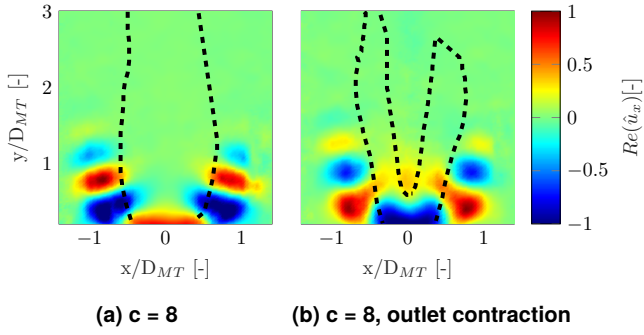


FIGURE 9: NORMALIZED TRANSVERSAL VELOCITY COMPONENT \hat{u}_x (REAL PART) FROM THE SPOD MODE 1, DASHED LINES INDICATE ZERO u_y LINE

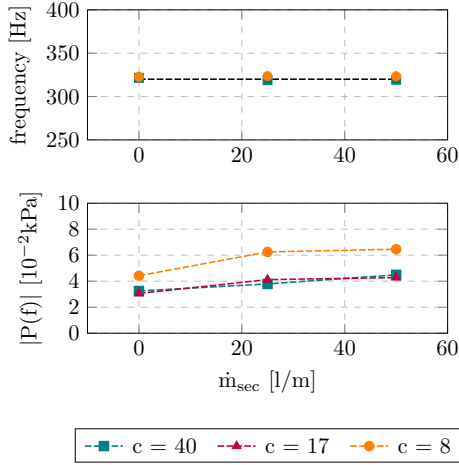


FIGURE 10: PVC FREQUENCIES AND PRESSURE AMPLITUDE FOR THE DUAL-STAGE SWIRLER IN DIFFERENT CONFINEMENT RATIOS WITH VARYING \dot{m}_{sec}

Fig. 10 shows the pressure amplitude and the PVC frequency in different confinement ratios for counter-rotating swirlers, in the configuration without exit nozzle. The frequency is independent of the confinement ratio and \dot{m}_{sec} , and therefore still scales with $St_{PVC} = 0.78$. This indicates that the PVC is mainly determined by the primary swirler, and it is formed in the mixing tube or just downstream of the mixing tube outlet, where the influence of the secondary swirler is still weak.

However, the amplitude of the pressure fluctuation increases with increasing \dot{m}_{sec} . For all confinement ratios, the pressure amplitude for the condition with $\dot{m}_{sec} = 50$ l/m is higher than the single swirler only. This indicates that the secondary mass flow does not dampen the strength of the PVC, but rather that the PVC imposes its frequency on the additional mass flow, consequently decreasing the amplitude of pressure fluctuations.

However, in Section 3.1.3, it was shown that the nozzle at the exit also affects the streamwise velocity and length of the jet forming in the forward direction. Therefore, the effect of the secondary mass flow rate injection \dot{m}_{sec} is here verified with and without the nozzle. Fig. 11 shows the average flow fields for $\dot{m}_{prim} = 250$ l/m and $\dot{m}_{sec} = 50$ l/m. Compared with the

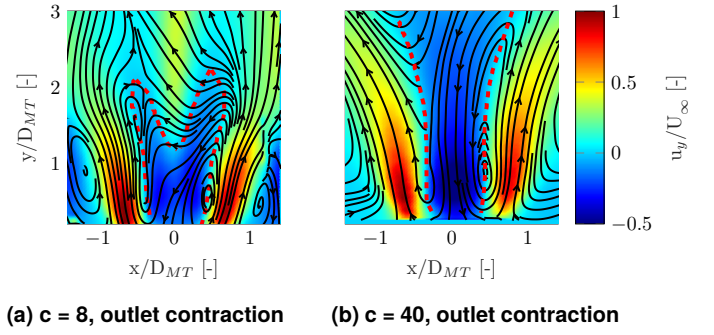


FIGURE 11: AVERAGE STREAMWISE u_y VELOCITY FIELDS WITH \dot{m}_{sec} , DASHED LINES INDICATES ZERO u_y LINE

flow fields where no \dot{m}_{sec} is present (Fig. 8c and 8d), the case with \dot{m}_{sec} shows a weaker and shorter influence of the outlet contraction on the flow field.

This is a result of the faster swirl decay for the counter-rotating configuration, which results in a lower effective swirl number at the outlet. As mentioned before, the effective swirl number at this location is one of the main parameters which determine the disturbance of the flow field [37]. This makes it difficult to evaluate a priori whether the change in PVC characteristics is a direct consequence of the secondary mass flow or an indirect one from the change in the influence of the outlet boundary condition. To isolate these effects, measurements were performed for $c = 40$ without outlet contraction. Fig. 12 shows the PVC frequency dependency on the mass flow going through the primary and the secondary swirler. The frequency is almost independent of the mass flow going in the outer swirler, thus it scales again with $St_{PVC} = 0.78$. The pressure amplitude for the dual swirler with $\dot{m}_{sec} = 75$ l/m increases linearly with the primary mass flow \dot{m}_{prim} . As previously discussed, the case with only primary mass flow shows an increasing trend for the amplitude until 250 l/m and drops slightly afterward. The highest \dot{m}_{sec} case results in the highest pressure amplitude. This implies that the mass flow in the counter-rotating swirler is indeed not dampening the PVC, but rather gets excited at the same frequency. For all the measured mass flow rates apart from $\dot{m}_{prim} = 250$ l/m, adding \dot{m}_{sec} either increases the pressure amplitude or keeps the amplitude constant. This indicates that the increase in PVC strength with increasing \dot{m}_{sec} is not a result of the outlet boundary condition but is directly related to the secondary mass flow. However, for $\dot{m}_{prim} = 250$ l/m this hypothesis can not be confirmed. While adding a low mass flow rate in the secondary air stream decreases the amplitude, it increases significantly for the addition of a high mass flow rate. While this particular case is protruding, the authors can not provide a plausible explanation at this stage of the research.

3.3 Axial air injection

The effect of axial air injection in the PVC modes is analyzed in this section. The previous sections showed that the outlet boundary condition does not affect the PVC frequencies. Therefore, the effect of AAI is only shown for the open exit configuration without outlet nozzle.

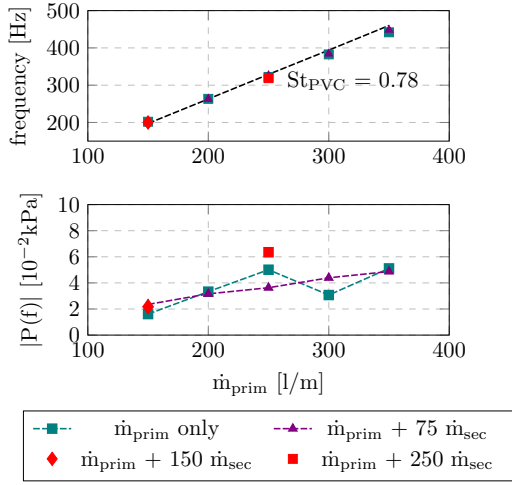


FIGURE 12: PVC FREQUENCIES AND PRESSURE AMPLITUDES FOR THE DUAL-STAGE SWIRLER AT DIFFERENT \dot{m}_{prim} , $C = 40$

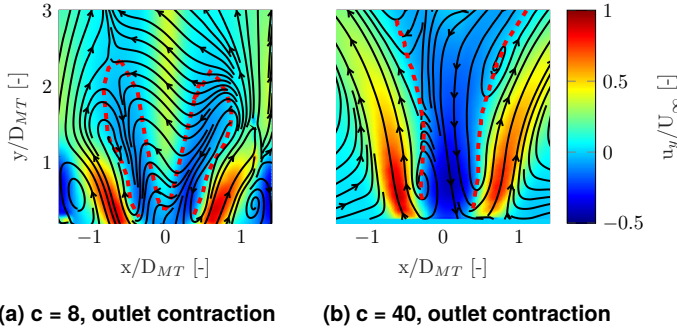


FIGURE 13: AVERAGE STREAMWISE u_y VELOCITY FIELDS WITH 10% χ , DASHED LINES INDICATES ZERO u_y LINE

Fig. 13 shows the influence of the AAI jet on the overall flow field. The total air mass flow is kept constant at $\dot{m}_{air} = 250$ l/m and the AAI fraction is varied according to Eq. 3. Due to AAI, the effective swirl number as defined in Eq. 1 decreases due to the redistribution of the axial flux of angular momentum and axial flux of tangential momentum. This results in a lower opening angle of the swirling jet and lower negative velocities in the IRZ compared to the case without AAI (see Fig. 8b and Fig. 13b). Fig. 14 shows the effect of AAI on the PVC frequency and the pressure amplitude for different confinement ratios. The frequencies obtained from the pressure measurements decrease with increasing χ , which is expected due to the consequent decrease in mass flow exiting the swirler. The graph additionally shows the $St_{PVC} = 0.78$ line, which is evaluated from the formula $St_{PVC} = \frac{f \cdot D_{MT}}{U_\infty}$ by using only swirling mass flow rate instead of the total mass flow rate for the calculation of U_∞ . One can observe that the frequency is not following $St_{PVC} = 0.78$ scaling, but shows a higher slope for the frequency decrease. As shown in Manoharan *et al.* [7], the PVC frequency scales linearly with the swirl number. Introducing AAI has a non-linear effect on the reduction of the swirl number [28], with a higher reduction of the swirl number for high percentages of χ . Therefore it is reasonable that the PVC frequency deviates more

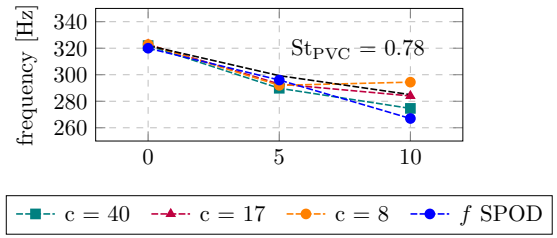


FIGURE 14: PVC FREQUENCIES AND PRESSURE AMPLITUDE FOR THE DUAL-STAGE SWIRLER IN DIFFERENT CONFINEMENT RATIOS WITH VARYING χ

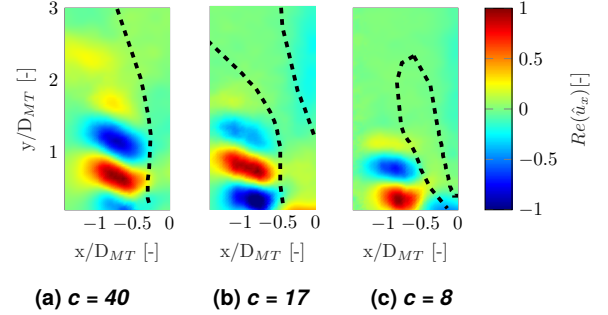


FIGURE 15: NORMALIZED TRANSVERSAL VELOCITY COMPONENT \hat{u}_x (REAL PART) FROM THE SPOD MODE 1, DASHED LINES INDICATES ZERO u_y LINE

from the constant St_{PVC} line for higher χ . It is also to be noted, that for the low percentage of χ (5%) the frequencies obtained by the pressure measurements are similar for all three confinement ratios. The frequency results in $St_{PVC} = 0.73$. For the higher percentage (10%) there is a discrepancy of 20 Hz between $c = 40$ and $c = 8$ for the frequencies obtained from the pressure signal. As expected, the PVC frequencies obtained by SPOD are similar for all c and therefore are only represented as one line. For $\chi = 10\%$, the SPOD frequency results in $St_{PVC} = 0.65$.

The SPOD frequencies match with the measured frequencies for $\chi = 0\%$ and $\chi = 5\%$. For the highest AAI ($\chi = 10\%$) the SPOD frequency is lower than the measured frequencies for all c . The cases with high AAI are the only measurement points, where the frequency obtained by pressure measurements does not match the one obtained by SPOD. This indicates, that there is a frequency increase from the PVC frequency to the one measured in the ORZ. The reason for this is unclear until this point and will be the objective of further investigations.

Fig. 15 shows the first SPOD mode at the PVC frequency for $\chi = 10\%$. It can be noted that the shape of the PVC is significantly different for $c = 40$ and $c = 17$ compared to the case with $\chi = 0\%$ (see Fig. 6). The opening angle is smaller and resembles more the pattern of the unconfined case. This a result of the change in opening angle of the swirling jet, as shown in Fig. 13. The PVC structure in the flow field of the smallest confinement ratio $c = 8$ however, does not show a significant influence of the AAI.

4. CONCLUSION

This study investigates the effect of the different geometric parameters on the precessing vortex core dynamics in a sin-

gle and dual-stage counter-rotating swirler. This work therefore contributes to understand and predict the PVC dynamics in unconventional combustion chamber geometries, which might be required when introducing alternative fuels like hydrogen. Pressure measurements and time-resolved PIV measurements show that the PVC scales with $St_{PVC} = 0.78$ based on the mass flow in the primary swirler, as expected from the literature. With this study, it is demonstrated that this scaling is independent of the mass flow in the secondary swirler. This indicates that the secondary counter-rotating mass flow does not influence the periodic phenomena generated in the primary swirler. Additionally, this work demonstrates that in the cases with axial air injection the PVC frequency does not scale directly with Strouhal number, as the effective swirl number is non-linearly changed with the addition of AAI. The pressure amplitude of the PVC, on the other side, is highly dependent on the investigated configuration. For the single stage, the smallest combustion chamber diameter shows the highest amplitude, both in the pressure measurements and in the modal energy of the PVC mode obtained by SPOD. The outer recirculation zone is small, which results in a large recirculated mass flow in the IRZ, which avoids the weakening of the PVC structure. For the dual-stage swirler, increasing the mass flow in the secondary swirler while keeping the one in the primary swirler constant increases the amplitude of the pressure fluctuations in most of the cases. This implies that the PVC imposes its frequency on the secondary mass flow and consequently increases the pressure fluctuations at that frequency. The results obtained from this study contribute to the understanding of the PVC dynamics in different combustor geometries. For the reacting cases in a single-stage configuration, previous works have reported linear relation (constant St_{PVC}) of the PVC frequency with increasing power at the same equivalence ratio [42]. This is expected to be applicable to this burner geometry as well. In future reacting flow experiments in this burner, the PVC dynamics will be investigated to assess the interaction of the PVC with the flame and verify the scaling of these findings in non-reacting conditions to reacting conditions. These investigations are expected to shed light on the stability limits of the combustor.

ACKNOWLEDGMENTS

This project has been financed by the Dutch Ministry of Economic Affairs and Climate under the TKI scheme (Grant number TKI HTSM/18.0170) along with SAFRAN Aircraft Engines and Airbus.

REFERENCES

- [1] Lieuwen, T.C. and Yang, V. *Combustion Instabilities in Gas Turbine Engines: Operational Experience, Fundamental Mechanisms and Modeling*. Progress in Astronautics and A, American Institute of Aeronautics and Astronautics (2005). URL https://books.google.nl/books?id=4_pTAAAAMAAJ.
- [2] Lucca-Negro, O. and O'Doherty, Tim. "Vortex Breakdown: a review." *Progress in Energy and combustion Science* Vol. 27 (2001): pp. 431–481. DOI [https://doi.org/10.1016/S0360-1285\(00\)00022-8](https://doi.org/10.1016/S0360-1285(00)00022-8).
- [3] Merkle, Klaus., Haessler, H., Büchner, Horst and Zarzalis, Nikolaos. "Effect of co- and counter-swirl on the isothermal flow- and mixture-field of an airblast atomizer nozzle." *International Journal of Heat and Fluid Flow* Vol. 24 No. 4 (2003): pp. 529–537. DOI [10.1016/S0142-727X\(03\)00047-X](https://doi.org/10.1016/S0142-727X(03)00047-X).
- [4] Hadeif, Redjem. and Lenze, Bernhardt. "Effects of co- and counter-swirl on the droplet characteristics in a spray flame." *Chemical Engineering and Processing: Process Intensification* Vol. 47 No. 12 (2008): pp. 2209–2217. DOI [10.1016/j.cep.2007.11.017](https://doi.org/10.1016/j.cep.2007.11.017).
- [5] Syred, Nicholas. "A review of oscillation mechanisms and the role of the precessing vortex core (PVC) in swirl combustion systems." *Progress in Energy and combustion Science* Vol. 32 No. 2 (2006): pp. 93–161. DOI [10.1016/j.peccs.2005.10.002](https://doi.org/10.1016/j.peccs.2005.10.002).
- [6] Oberleitner, Kilian., Sieber, Moritz., Nayeri, Christian. N., Paschereit, Christian. O., Petz, Christoph., Hege, Hans-Christian., Noack, Bernd. R. and Wygnasnski, Israel. "Three-dimensional coherent structures in a swirling jet undergoing vortex breakdown: stability analysis and empirical mode construction." *Journal of Fluid Mechanics* Vol. 679 (2011): pp. 383–414. DOI [10.1017/jfm.2011.141](https://doi.org/10.1017/jfm.2011.141).
- [7] Manoharan, Kiran, Frederick, Mark, Clees, Sean, O'Connor, Jacqueline and Hemchandra, Santosh. "A weakly nonlinear analysis of the precessing vortex core oscillation in a variable swirl turbulent round jet." *Journal of Fluid Mechanics* Vol. 884 (2020): p. A29. DOI [10.1017/jfm.2019.903](https://doi.org/10.1017/jfm.2019.903).
- [8] Stöhr, Michael, Oberleithner, Kilian, Sieber, Moritz, Yin, Zhiyao and Meier, Wolfgang. "Experimental Study of Transient Mechanisms of Bi-Stable Flame Shape Transitions in a Swirl Combustor." *ASME Turbo Expo 2017: Turbine Technical Conference and Exposition*. GT2017-65003. June 26–30, 2017. Charlotte, North Carolina, USA. DOI [10.1115/GT2017-65003](https://doi.org/10.1115/GT2017-65003). URL <https://asmedigitalcollection.asme.org/GT/proceedings-abstract/GT2017/50855/V04BT04A063/242873>.
- [9] Oberleithner, Kilian, Stöhr, Michael, Im, Seong Ho, Arndt, Christoph M. and Steinberg, Adam M. "Formation and flame-induced suppression of the precessing vortex core in a swirl combustor: Experiments and linear stability analysis." *Combustion and Flame* Vol. 162 No. 8 (2015): pp. 3100–3114. DOI [10.1016/J.COMBUSTFLAME.2015.02.015](https://doi.org/10.1016/J.COMBUSTFLAME.2015.02.015).
- [10] Liang, Hanzhuang. and Maxworthy, Tony. "An experimental investigation of swirling jets." *Journal of Fluid Mechanics* Vol. 525 (2005): pp. 115–159. DOI [10.1017/S0022112004002629](https://doi.org/10.1017/S0022112004002629).
- [11] Litvinov, Ivan V., Shtork, Sergey I., Kuibin, Pavel A., Alekseenko, Sergey V. and Hanjalic, Kemal. "Experimental study and analytical reconstruction of precessing vortex in a tangential swirler." *International Journal of Heat and Fluid Flow* Vol. 42 (2013): pp. 251–264. DOI [10.1016/j.ijheatfluidflow.2013.02.009](https://doi.org/10.1016/j.ijheatfluidflow.2013.02.009).
- [12] Stöhr, Michael, Boxx, Isaac, Carter, Campbell and Meier, Wolfgang. "Experimental study of vortex-flame interaction in a gas turbine model combustor." *Combustion and Flame* Vol. 162 No. 8 (2015): pp. 3100–3114. DOI [10.1016/J.COMBUSTFLAME.2015.02.015](https://doi.org/10.1016/J.COMBUSTFLAME.2015.02.015).

- tion and Flame Vol. 159 (2012): p. 2636–2649. DOI [10.1016/j.combustflame.2012.03.020](https://doi.org/10.1016/j.combustflame.2012.03.020).
- [13] Steinberg, Adam M., Arndt, Christoph M. and Meier, Wolfgang. “Parametric study of vortex structures and their dynamics in swirl-stabilized combustion.” *Proceedings of the Combustion Institute* Vol. 34 No. 2 (2013): pp. 3117–3125. DOI [10.1016/j.proci.2012.05.015](https://doi.org/10.1016/j.proci.2012.05.015).
- [14] Zhang, Robert, Boxx, Isaac, Meier, Wolfgang and Slabaugh, Carson D. “Coupled interactions of a helical precessing vortex core and the central recirculation bubble in a swirl flame at elevated power density.” *Combustion and Flame* Vol. 202 (2019): pp. 119–131. DOI <https://doi.org/10.1016/j.combustflame.2018.12.035>.
- [15] Karmarkar, Ashwini, Gupta, Saarthak, Boxx, Isaac, Hemchandra, Santosh and O’Connor, Jacqueline. “Impact of precessing vortex core dynamics on the thermoacoustic instabilities in a swirl-stabilized combustor.” *Journal of Fluid Mechanics* Vol. 946 (2022). DOI [10.1017/jfm.2022.610](https://doi.org/10.1017/jfm.2022.610).
- [16] Lückoff, Finn and Oberleithner, Kilian. “Excitation of the precessing vortex core by active flow control to suppress thermoacoustic instabilities in swirl flames.” *International Journal of Spray and Combustion Dynamics* Vol. 11 (2019): p. 175682771985623. DOI [10.1177/1756827719856237](https://doi.org/10.1177/1756827719856237).
- [17] Manoharan, Kiran, Hansford, Samuel, O’Connor, Jacqueline and Hemchandra, Santosh. “Instability Mechanism in a Swirl Flow Combustor: Precession of Vortex Core and Influence of Density Gradient.” *ASME Turbo Expo 2015: Turbine Technical Conference and Exposition*. GT2015-42985. June 15–19, 2015. Montreal, Quebec, Canada. DOI [10.1115/GT2015-42985](https://doi.org/10.1115/GT2015-42985). URL <https://asmedigitalcollection.asme.org/GT/proceedings-abstract/GT2015/56680/V04AT04A073/237055>.
- [18] Stöhr, Michael., Arndt, Christoph. M. and Meier, Wolfgang. “Transient effects of fuel–air mixing in a partially-premixed turbulent swirl flame.” *Proceedings of the Combustion Institute* Vol. 35 No. 3 (2015): pp. 3327–3335. DOI [10.1016/j.proci.2014.06.095](https://doi.org/10.1016/j.proci.2014.06.095).
- [19] Terhaar, Steffen, Oberleithner, Kilian and Paschereit, Christian Oliver. “Impact of Steam-Dilution on the Flame Shape and Coherent Structures in Swirl-Stabilized Combustors.” *Combustion Science and Technology* Vol. 186 No. 7 (2014): pp. 889–911. DOI [10.1080/00102202.2014.890597](https://doi.org/10.1080/00102202.2014.890597).
- [20] Lückoff, Finn, Sieber, Moritz, Paschereit, Christian Oliver and Oberleithner, Kilian. “Impact of the Precessing Vortex Core on NO_x Emissions in Premixed Swirl-Stabilized Flames—An Experimental Study.” *Journal of Engineering for Gas Turbines and Power* Vol. 142 No. 11 (2020). DOI [10.1115/1.4048603](https://doi.org/10.1115/1.4048603).
- [21] Reichel, Thoralf G., Terhaar, Steffen and Paschereit, Oliver. “Increasing Flashback Resistance in Lean Premixed Swirl-Stabilized Hydrogen Combustion by Axial Air Injection.” *Journal of Engineering for Gas Turbines and Power* Vol. 137 No. 7 (2015). DOI [10.1115/1.4029119](https://doi.org/10.1115/1.4029119).
- [22] Reichel, Thoralf G. “Flashback Prevention in Lean Hydrogen Combustion.” Dissertation, Technische Universität Berlin, Berlin. 2017.
- [23] Syred, Nicholas. and Beér, János. M. “Combustion in swirling flows: A review.” *Combustion and Flame* Vol. 23 No. 2 (1974): pp. 143–201. DOI [10.1016/0010-2180\(74\)90057-1](https://doi.org/10.1016/0010-2180(74)90057-1).
- [24] Khalil, Ahmed E.E., Brooks, Jonathan M. and Gupta, Ashwani K. “Impact of confinement on flowfield of swirl flow burners.” *Fuel* Vol. 184 (2016): pp. 1–9. DOI <https://doi.org/10.1016/j.fuel.2016.06.098>.
- [25] Fu, Yongqiang, Jeng, San-Mou and Tacina, Robert. “Confinement Effects on the Swirling Flow Generated by a Helical Axial Swirler.” *44th AIAA Aerospace Sciences Meeting and Exhibit*. January 9-12, 2006. Reston, Virginia. DOI [10.2514/6.2006-545](https://doi.org/10.2514/6.2006-545).
- [26] Ji, Longjuan, Wang, Jinhua, Zhang, Weijie, Mao, Runze, Hu, Guangya and Huang, Zuohua. “Effect of confinement ratio on flame structure and blow-off characteristics of swirl flames.” *Experimental Thermal and Fluid Science* Vol. 135 (2022): p. 110630. DOI [10.1016/J.EXPTHERMFLUSCI.2022.110630](https://doi.org/10.1016/J.EXPTHERMFLUSCI.2022.110630).
- [27] Tong, Yiheng, Li, Mao, Thern, Marcus and Klingmann, Jens. “An Experimental Study of Effects of Confinement Ratio on Swirl Stabilized Flame Macrostructures.” *ASME 2017 Power Conference Joint With ICOPE-17 collocated with the ASME 2017 11th International Conference on Energy Sustainability, the ASME 2017 15th International Conference on Fuel Cell Science, Engineering and Technology, and the ASME 2017 Nuclear Forum*. POWER-ICOPE2017-3064. June 26–30, 2017. Charlotte, North Carolina. DOI [10.1115/POWER-ICOPE2017-3064](https://doi.org/10.1115/POWER-ICOPE2017-3064).
- [28] Terhaar, Steffen, Reichel, Thoralf G., Schrodinger, Christina, Rukes, Lothar, Oberleithner, Kilian and Paschereit, Christian O. “Vortex Breakdown and Global Modes in Swirling Combustor Flows with Axial Air Injection.” *43rd Fluid Dynamics Conference*. June 24-27, 2013. San Diego, CA. DOI [10.2514/6.2013-2602](https://doi.org/10.2514/6.2013-2602).
- [29] Spalding, Dudley. B. “Combustion Aerodynamics. By Beer, J. and Chigier, N.A., Applied Science Publishers Ltd, 1972. 264 pp.” *Journal of Fluid Mechanics* Vol. 54 No. 4 (1972): p. 762–762. DOI [10.1017/S0022112072210990](https://doi.org/10.1017/S0022112072210990).
- [30] Terhaar, S., Čosić, B., Paschereit, C. O. and Oberleithner, K. “Suppression and excitation of the precessing vortex core by acoustic velocity fluctuations: An experimental and analytical study.” *Combustion and Flame* Vol. 172 (2016): pp. 234–251. DOI [10.1016/j.combustflame.2016.06.013](https://doi.org/10.1016/j.combustflame.2016.06.013).
- [31] Schmidt, O. T. “Spectral proper orthogonal decomposition using multitaper estimates.” *Theoretical and Computational Fluid Dynamics* (2022): pp. 1–14 URL <https://rdcu.be/cUtP3>.
- [32] Weiss, Julien. “A Tutorial on the Proper Orthogonal Decomposition.” *AIAA Aviation 2019 Forum*. 2019. American Institute of Aeronautics and Astronautics, Reston, Virginia. DOI [10.2514/6.2019-3333](https://doi.org/10.2514/6.2019-3333).
- [33] Schmidt, Oliver and Colonius, Tim. “Guide to Spectral Proper Orthogonal Decomposition.” *AIAA Journal* Vol. 58 (2020): pp. 1–11. DOI [10.2514/1.J058809](https://doi.org/10.2514/1.J058809).
- [34] Mason, Danielle, Clees, Sean, Frederick, Mark and O’Connor, Jacqueline. “The Effects of Exit Boundary Con-

- dition on Precessing Vortex Core Dynamics.” *ASME Turbo Expo 2019: Turbomachinery Technical Conference and Exposition*. GT2019-91079. June 17–21, 2019. Phoenix, Arizona. DOI [10.1115/GT2019-91079](https://doi.org/10.1115/GT2019-91079). URL <https://asmedigitalcollection.asme.org/GT/proceedings-abstract/GT2019/58622/V04BT04A009/1066781>.
- [35] Anand, Vijay, Jodele, Justas, Prisell, Erik, Lyrsell, Owe and Gutmark, Effie. “Dynamic Features of Internal and External Flowfields of Pulsejet Engines.” *AIAA Journal* Vol. 58 (2020). DOI [10.2514/1.J059685](https://doi.org/10.2514/1.J059685).
- [36] Favrel, Arthur, Liu, Zhihao and Miyagawa, Kazuyoshi. “Enhancing effect of an open pipe exit on the precessing vortex core occurring in confined swirling flows.” *Experiments in Fluids* Vol. 61 (2020): p. 211. DOI [10.1007/s00348-020-03042-1](https://doi.org/10.1007/s00348-020-03042-1).
- [37] Terhaar, Steffen, Bobusch, Bernhard C. and Paschereit, Christian Oliver. “Effects of Outlet Boundary Conditions on the Reacting Flow Field in a Swirl-Stabilized Burner at Dry and Humid Conditions.” *ASME Turbo Expo 2012: Turbine Technical Conference and Exposition*. GT2012-69753: pp. 1295–1306. June 11–15, 2012. Copenhagen, Denmark. DOI [10.1115/GT2012-69753](https://doi.org/10.1115/GT2012-69753). URL <https://asmedigitalcollection.asme.org/GT/proceedings-abstract/GT2012/44687/1295/250502>.
- [38] Li, Guoqiang and Gutmark, Ephraim J. “Effect of exhaust nozzle geometry on combustor flow field and combustion characteristics.” *Proceedings of the Combustion Institute* Vol. 30 No. 2 (2005): pp. 2893–2901. DOI [10.1016/j.proci.2004.08.189](https://doi.org/10.1016/j.proci.2004.08.189).
- [39] Grundmann, Sven, Wassermann, Florian, Lorenz, Ramona, Jung, Bernd and Tropea, Cameron. “Experimental investigation of helical structures in swirling flows.” *International Journal of Heat and Fluid Flow* Vol. 37 (2012): pp. 51–63. DOI [10.1016/j.ijheatfluidflow.2012.05.003](https://doi.org/10.1016/j.ijheatfluidflow.2012.05.003).
- [40] Escudier, Michael. P. and Keller, J. J. “Recirculation in swirling flow - A manifestation of vortex breakdown.” *AIAA Journal* Vol. 23 No. 1 (1985): pp. 111–116. DOI [10.2514/3.8878](https://doi.org/10.2514/3.8878).
- [41] Shakeel, Raghieb and Mokheimer, Esmail. “Swirl flow in annular geometry with varying cross-section.” *Engineering Applications of Computational Fluid Mechanics* Vol. 16 (2022): pp. 1154–1172. DOI [10.1080/19942060.2022.2076744](https://doi.org/10.1080/19942060.2022.2076744).
- [42] Oberleithner, Kilian, Terhaar, Steffen, Rukes, Lothar and Paschereit, Christian Oliver. “Why Non-Uniform Density Suppresses the Precessing Vortex Core.” *Volume 1B: Combustion, Fuels and Emissions*. 2013. American Society of Mechanical Engineers. DOI [10.1115/GT2013-95509](https://doi.org/10.1115/GT2013-95509).